Highlights

MIB adsorbed on SPAC was desorbed by NOM up to the adsorption equilibrium

MIB adsorbed on conventionally sized PAC was partially desorbed

MIB adsorption on SPAC was more reversible than on PAC

Irreversible adsorption was caused by pore blockage on the PAC particle surface

We observed external adsorption on a PAC particle by using ^{15}N-labeled EfOM

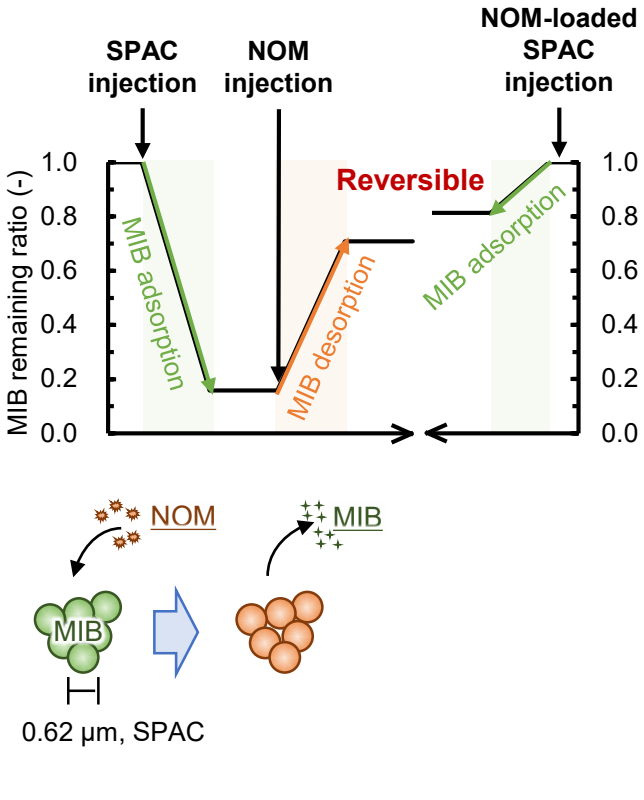
SPAC injection
NOM injection
NOM-loaded SPAC injection
MIB remaining ratio (-)
1.0
0.8
0.6
0.4
0.2
0.0
Reversible
MIB adsorption
MIB desorption
MIB adsorption
NOM
MIB
MIB
0.62 μm, SPAC

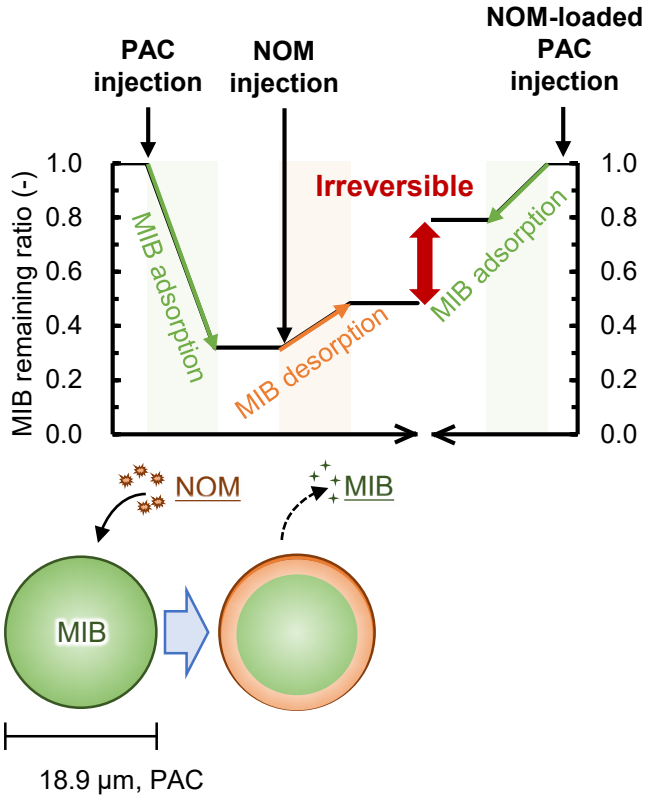
PAC injection
NOM injection
NOM-loaded PAC injection
MIB remaining ratio (-)
1.0
0.8
0.6
0.4
0.2
0.0
Irreversible
MIB adsorption
MIB desorption
MIB adsorption
NOM
MIB
MIB
18.9 μm, PAC

Effects of Pre, Post, and Simultaneous Loading of Natural Organic Matter on 2-Methylisoborneol Adsorption on Superfine Powdered Activated Carbon: Reversibility and External Pore-blocking

Akiko Nakayama[1], Asuka Sakamoto[1], Taku Matsushita[2], Yoshihiko Matsui[2,*], and Nobutaka Shirasaki[2]

[1]Graduate School of Engineering, Hokkaido University

[2]Faculty of Engineering, Hokkaido University

* Corresponding author. Phone: +81-11-706-7280.

E-mail address: matsui@eng.hokudai.ac.jp

ABSTRACT

Three different natural organic matter (NOM)-loading methods were compared for the adsorptive removal of 2-methylisoborneol (MIB) by superfine powdered activated carbon (SPAC) and conventionally-sized powdered activated carbon (PAC). The three NOM-loading methods were: NOM adsorption followed by MIB (MIB adsorption on NOM-preloaded carbon), MIB adsorption followed by NOM (MIB adsorption on NOM post-loaded carbon), and simultaneous NOM and MIB loading (MIB adsorption on NOM-simultaneously loaded carbon). MIB removals were similar for the smaller-sized carbon (SPAC) at higher AC dosages and at lower initial NOM concentrations. The similar MIB removals indicate direct site competition between MIB and NOM with MIB adsorption reversibility (complete desorption of MIB by NOM). At lower AC doses, especially for PACs, and at higher initial NOM concentrations, the adsorption of MIBs depended on the sequence of MIB or NOM adsorption. MIB removal was lowest for the NOM-preloaded carbon, followed by NOM-simultaneously loaded carbon. The highest MIB removal was achieved by post-loading of NOM, indicating that the adsorption is irreversible. MIB adsorption on SPAC was more reversible than on PAC, although the pore size distributions of the two carbons were similar. The high degree of adsorption irreversibility for PAC compared with SPAC indicated that pore blocking occurs due to NOM loading at the PAC particle surface. Images of the external adsorption were obtained using isotope mapping and ^{15}N-labeled effluent organic matter.

KEYWORDS

PAC; particle size; sub-micrometer; competitive adsorption; humic substance; taste and odor

1. Introduction

The ubiquity, abundance, and diversity of natural organic matter (NOM) in water sources is important for evaluating activated carbon (AC) adsorption for treating micropollutants. Micropollutant adsorption capacity decreases upon NOM loading compared to the initial capacity. The NOM effect on micropollutant adsorption originates from the direct competition for adsorption sites or by pore blockage (Summers et al. 2011). Direct competition occurs when competing compounds are of the same size, can access and compete for the same sites. Direct competition is the dominant mechanism of the NOM effect when the NOM loading level is below a certain threshold (Ding et al. 2006, Kilduff et al. 1998). Therefore, for the simultaneous removal of micropollutants and NOM in batch adsorption systems where the NOM loading is low, NOM marginally affects the internal diffusion of micropollutants in an AC particle, although NOM severely affects the adsorptive capacity of micropollutants (Cook et al. 2001, Huang et al. 1996, Matsui et al. 2003). Micropollutant adsorption capacity models in the presence of NOM have been developed to predict micropollutant removal, but are based on the direct competition mechanism, and reversible adsorption-desorption is implicitly assumed (Knappe et al. 1998, Najm et al. 1990, Zoschke et al. 2011). Experimental tests of simultaneous adsorption of target compounds and NOM have been reported, and previously developed models have been successfully verified. However, it remains unclear whether the NOM effect is truly reversible and whether the sequence of NOM/micropollutant loading affects adsorptive removal. Adsorption test of target compounds using adsorbent preloaded with NOM has not been applied in many of the landmark studies (Kilduff et al. 1998, Kilduff and Wigton 1999).

Studies using NOM-preloaded AC mostly aimed to elucidate pore blocking mechanisms by determination of adsorption/desorption and irreversibility (Karanfil et al. 2006, Pelekani and Snoeyink 1999, Pelekani and Snoeyink 2000, To et al. 2008). Preloaded NOM does not desorb to a measurable extent (Kilduff and Wigton 1999, Summers and Roberts 1988), but this does not necessarily indicate that micropollutants fail to displace pre-adsorbed NOM because of the inability to detect the extremely

low NOM concentrations desorbed. In contrast, a preloaded micropollutant (a pesticide, atrazine) was displaced by NOM, while preloading with NOM showed adsorption capacity reduction compared with the simultaneous adsorption of NOM and atrazine (Pelekani and Snoeyink 1999). The authors attributed this phenomenon to direct site adsorption competition in secondary micropores that can be accessed by both atrazine and NOM. Competitive adsorption between atrazine and model compounds also showed that preloaded atrazine can be displaced from secondary micropores to a larger extent than from primary micropores by model compounds (Pelekani and Snoeyink 2000, 2001). The authors also showed the adsorption reversibility of atrazine. However, atrazine adsorption capacities are not equivalent between the three types of ACs: NOM-preloaded AC, AC with preloaded atrazine followed by displacement by NOM, and AC simultaneously loaded by NOM and atrazine, and complete reversibility was not observed. On the primarily microporous AC, the uptake of atrazine in the presence of NOM (simultaneous adsorption) was comparable to the NOM-preloaded capacity. In addition, preloaded atrazine was not displaced by the subsequently adsorbed NOM. These results were attributed to pore blockage wherein NOM molecules block access to, but do not penetrate into, the primary micropores. When the AC preloaded with atrazine was dosed into NOM water, the amount of atrazine displaced by NOM increased with decreasing AC dosage, which increased NOM loading (Li et al. 2002). Very recently, Aschermann et al. (2018) reported that micropollutant desorption by NOM is dependent on the pore sizes. Macroporous AC shows a higher degree of desorption than microporous AC because pore blockage effects are minor (Aschermann et al. 2019).

However, apart from these studies, investigations of the pore blockage mechanisms have focused on partial pore blocking and pore constriction wherein adsorption kinetics decrease through internal diffusion (Ding et al. 2006, Ding et al. 2008, Li et al. 2003a, Li et al. 2003b, To et al. 2008) rather than complete pore blocking which lowers adsorption reversibility. The extent of displacement reversibility remains unclear, namely whether the micropollutant remained on the AC after displacement by NOM is larger than or the same as that obtained on the NOM-preloaded AC.

90 The effect of adsorbent particle size in the sub-micrometer range on micropollutant removal has been
91 recently investigated (Cai et al. 2013, Delgado et al. 2012, Ellerie et al. 2013, Huang et al. 2009, Matsui
92 et al. 2004, Wang et al. 2011). Superfine powdered activated carbon (SPAC) adsorbs NOM more
93 effectively and is loaded highly with NOM compared to conventionally-sized powdered activated
94 carbon (PAC) at a given AC dosage (Ando et al. 2010). However, the higher NOM loading on SPAC
95 relative to PAC does not result in a decrease in the adsorption capacity for a micropollutant beyond
96 that obtained for PAC. This phenomenon can be explained by the localization of NOM loading in an
97 AC particle. Different effects of NOM between SPAC and PAC are expected on micropollutant uptake-
98 displacement.

99 Herein, SPAC and PAC were used as adsorbents and 2-methylisoborneol (MIB), a major organic
100 micropollutant responsible for undesirable taste and odor at much less than μg/L levels for many water
101 utilities, was used as the target molecule. To investigate the reversibility of MIB adsorption-desorption
102 in the presence of NOM, MIB adsorption tests were performed under three conditions: adsorption of
103 NOM followed by MIB (NOM preloading), simultaneous MIB and NOM adsorption (NOM
104 simultaneous-loading), and adsorption of MIB followed by NOM (NOM post-loading).

105

106 **2. Materials and Methods**

107 2.1. *Activated carbon*

108 Commercially available wood-based PAC (Taikou-W, Futamura Chemical Industries Co., Gifu, Japan)
109 was obtained, prepared as a slurry in ultrapure water (Milli-Q Advantage, Millipore Co.), and milled
110 to superfine particles using a wet bead mill (LMZ015, Ashizawa Finetech, Chiba, Japan). Herein, the
111 as-received PAC is referred to as PAC, and the milled activated carbons as SPAC. The ACs were stored
112 as slurries in ultrapure water at 4 °C and used after dilution and vacuum treatment. The AC particle
113 size distributions were determined using a laser-light-scattering instrument (Microtrac MT3300EXII,

Nikkiso Co., Tokyo, Japan) after dispersant addition (Triton X-100, Kanto Chemical Co., Tokyo, Japan; final concentration, 0.08 vol%) and subsequent ultrasonic dispersion. The median diameters of PAC and SPAC were 18.9 and 0.62 μm, respectively, unless otherwise stated. The pore size distributions were determined using the nitrogen gas adsorption-desorption method (Autosorb-iQ, Quantachrome Instruments, Kanagawa, Japan).

2.2. *Water samples*

Water containing natural organic matter (NOM) was prepared by dissolving Suwannee River humic acid (SHA) and fulvic acid (SFA; International Humic Substance Society) in ultrapure water containing inorganic ions. The ion compositions of the prepared samples were the same as that used in a previous study (Ando et al. 2010). Besides these NOM water samples, natural water samples containing NOM were collected from the Chibaberi River (Hokkaido, Japan). The water was filtered through a 0.2 μm PTFE membrane (DISMIC-25HP; Toyo Roshi Kaisha, Ltd., Tokyo) to remove any undissolved NOM. The dissolved organic carbon (DOC) concentration and absorbance at 260 nm (UV260) were used as parameters for bulk NOM quantification (TOC: Model 810; Sievers 900, Ionics Instrument Business Grp., Boulder Co.; UV260: UV-1800, Shimadzu Co., Kyoto, Japan).

Stock solutions of MIB were prepared by dissolving reagent pure MIB (Wako Pure Chemical Industries, Osaka, Japan) in ultrapure water and filtering the resulting solution through a 0.2 μm PTFE membrane filter. Single solute solutions of MIB were prepared by diluting the MIB stock solution with NOM-free water, which were prepared with ultrapure water containing inorganic ions added to make the ionic composition equal to those of the SFA and SHA water samples. Solutions of MIB in NOM-containing water were prepared by diluting MIB with the SFA, SHA, and Chibaberi waters. MIB concentrations were adjusted to 1000 ng/L unless otherwise stated. MIB concentrations were analyzed

using a Purge and Trap Concentrator (OI Analytical/Xylem Inc., TX, USA) coupled to a GC-MS (789 GC + 5975 MSD, Agilent Technologies Japan, Tokyo) using ^{2}H-labeled geosmin (Hayashi Pure Chemical Ind., Ltd., Osaka, Japan) as an internal standard.

2.3. *Batch adsorption tests*

Equilibrium removals of MIB in the presence/absence of NOM were examined by five tests as follows:

1) *NOM simultaneous-loading tests*. Aliquots (150 mL) from 1 or 3 L solutions containing both MIB (1000 ng/L) and NOM (0.9 to 7 mg-C/L) were transferred to vials. A specified amount of SPAC/PAC was added, and the vials were immediately shaken by hand vigorously and transferred to a shaker for two weeks of mixing at a constant temperature of 20 °C.

2) *NOM post-loading test*. After adding a specified amount of SPAC/PAC to vials containing 140 mL of MIB solution, the samples were vigorously shaken by hand and transferred to a shaker for one week of shaking at a constant temperature of 20 °C. Afterward, a small amount of high concentration NOM (SFA or SHA) solution (10 mL, 12 to 90 mg-C/L) was added to the vial to bring the initial DOC concentration to the same level as those used in the NOM simultaneous-loading test. After vigorous shaking by hand, the vials were returned to the shaker for one week of mixing. The NOM post-loading test of the Chibaberi water samples was conducted by adding SPAC/PAC to vials containing a MIB solution of 2000 ng/L. After shaking the vials for one week, Chibaberi water (DOC: 3.4 mg-C/L) was added at 1:1 vol/vol ratio for final MIB and DOC concentrations of 1000 ng/L and 1.7 mg/L, respectively. After vigorous shaking by hand, the vials were returned to the shaker for mixing for one week.

3) *NOM preloading test*. The procedure of the NOM preloading test was the opposite of the NOM post-loading test. After adding a specified amount of SPAC/PAC to vials containing 140 mL of the

NOM solution and shaking the vials for one week, a small amount of high concentration MIB solution (10 mL, 15 μg/L) was added to the vial containing the NOM-preloaded AC to bring an initial MIB concentration of approximately 1000 ng/L. The vials were subsequently shaken for two weeks.

4) *Single MIB test*. MIB removal in the absence of NOM was examined using the same procedure as for the NOM simultaneous-loading tests except that the solution did not contain NOM.

5) *Preloading-pulverization test*. After a specified amount of PAC was added to a bottle containing a 1.5-mg/L NOM solution (5 L), the bottle was shaken and transferred to a shaker for one week of mixing for adsorption. After shaking, the PAC was recovered and pulverized by the following procedure. The bottle was kept at rest for 3 days for the PAC particles to settle to the bottom. The top 4.5 L of the water (supernatant) was discarded. The remaining water containing NOM-loaded PAC particles was centrifuged at 1000 rpm (133 g) for 60 min, and the upper part was carefully discarded to reduce the volume containing PAC particles to 10 mL. The water containing the PAC particles was transferred to a mortar and placed under vacuum for 3 h to evaporate most of the remaining water. Afterward, the wet PAC particle sludge was obtained, which was then pounded by a pestle for 10 min for fracturing. The particle sizes of the PACs before and after fracturing were determined using a laser light-scattering instrument. A portion of the sludge containing the fractured PAC was added to a vial containing 140 mL of water (MIB concentration of 1000 ng/L, same ionic composition as the NOM water) at a concentration of 1.5 mg/L. The PAC sludge before fracturing was added to a vial to prepare a control sample. The vials were shaken for two weeks.

According to a previous report (Matsui et al. 2013), MIB adsorption equilibrium can be reached within one week, and NOM adsorption nearly reached equilibrium. However, internal diffusion of the desorbed compound by displacement in an AC particle may slow (To et al. 2008). Therefore, it was previously confirmed in long-term shaking tests that after two weeks of MIB contact, adsorption equilibrium could be reached. In the long-term shaking tests, MIB removal ratios were unchanged

between two and three weeks of MIB contact time (see Fig. 1S in the Supplementary Information). Therefore, an AC-water contact time of ≥ two weeks was used. Control tests were also conducted using multiple bottles that did not contain AC to confirm that concentration changes during long-term mixing were negligible without the adsorbent. After the water samples were filtered through a 0.2 μm PTFE membrane filter, the MIB and NOM concentrations in the water phase were measured.

2.5. *Isotope microscopy of the internal adsorption profile*

^{2}H-labeled MIB was obtained from Wako Pure Chemical Industries, and ^{15}N-labeled EfOM (effluent organic matter) was produced via the following procedure. Activated sludge sampled from a wastewater treatment plant (Soseigawa, Sapporo, Japan) was injected into M9 minimal medium containing ^{15}N-labeled NH_4Cl and natural NH_4Cl at a 1:1 ratio, and subsequently cultured by adding glucose every day. After culturing for 16 days, the water was filtered through a 0.45 μm pore size mixed cellulose ester (MCE) membrane to remove the activated sludge and then filtered through ultrafiltration membranes with a nominal MW cutoff of 10 kD (regenerated cellulose membrane, PLGC04310, Millipore). Most of the ammonia remained in the water was removed by air stripping at pH 12. After returning pH to 7, the water was filtered through ultrafiltration membranes with nominal MW cutoff of 1 kDa (regenerated cellulose membrane, PLAC04310, Millipore) in order to separate EfOM from ammonia. The membrane retentate containing EfOM was obtained. The $^{15}N/^{14}N$ ratio of the EfOM was 0.018, markedly higher than the natural $^{15}N/^{14}N$ ratio of 0.0030.

PAC particles that adsorbed ^{2}H-labeled MIB and ^{15}N-labeled EfOM were obtained using the adsorption procedures described in Section 2.3. Only the conventionally-sized PAC was used for isotope microscopy analysis because the image resolution was not sufficient to visualize adsorption profiles in the SPAC particles. After adsorption, the waters were filtered through a 0.2-μm alumina membrane (Spectrum Chemical Mfg. Corp., USA) covered with a 100-nm thick gold layer produced by gold

209 evaporation, and PAC particles were collected on the membrane. Gold evaporation was conducted to
210 improve conductivity and prevent the membrane from becoming charged during the isotope
211 microscopy measurements. After the particles on the membrane were imaged using a low vacuum
212 scanning electron microscope (LV-SEM; JSM-6360LA, JEOL), the intensities of ^{2}H, ^{1}H, ^{15}N, and ^{14}N
213 on the AC particles were observed as a two-dimensional map using an isotope microscope system
214 (Hokkaido University, Sapporo, Japan). Details of the observation procedure are described elsewhere
215 (Matsui et al. 2014). The $^{2}H/^{1}H$ ratios were calculated on the spots that had sufficient ^{1}H detection
216 signal intensities in the maps to estimate the intraparticle MIB distributions, while $^{15}N/^{14}N$ ratios were
217 calculated on the spots with sufficient ^{14}N signal intensities to estimate the intraparticle EfOM
218 distributions.

219

220 ## 3. Results and Discussion

221 ### 3.1. *Comparison of MIB removal*

222 Proportions of MIB remaining (C/C_0) are plotted against AC dosages in Figs. 1–3. The proportions of
223 MIB remaining were higher in the presence of NOM compared to those without NOM (single
224 adsorbate system). Of all three tests in the presence of NOM, the proportion of MIB remaining was
225 the highest on the NOM-preloaded AC and lowest on the NOM-post-loaded AC. However, the
226 difference in the proportions of MIB remaining in the three tests was small at high AC dosages of >10
227 mg/L. A small difference was also observed at low AC dosages for SPAC when the initial NOM
228 concentration was low (left panel of Fig. 1 and upper left panels of Figs. 2 and 3).

229 When ACs were added to the NOM-free MIB water and shaken for two weeks to equilibrate, MIB
230 concentrations corresponding to the proportion of remaining were obtained, as shown in the diamond
231 plots in Figs. 1–3. When water samples where MIB had previously been equilibrated were spiked with
232 NOM and shaken for another week, the MIB concentrations increased and became higher than that

before spiking NOM (the diamond plots moved to the circle plots in Figs. 1–3). This indicated that the preloaded MIB was desorbed back to the water phase by the displacement with NOM. Therefore, the fact that the proportion of MIB removal by post-loaded AC was the same as that by NOM-preloaded AC can be interpreted as the complete reversibility of MIB adsorption. Furthermore, since adsorption reversibility is not expected when pore blocking occurs, it is presumed that the NOM effect was caused by direct site competition (Matsui et al. 2012, Newcombe et al. 1997).

Similar proportions of MIB removals for the NOM-preloaded AC, NOM-post-loaded AC and NOM-simultaneously loaded AC indicate that the displacement of preloaded MIB occurred until the equilibrium of the competitive MIB and NOM adsorption was reached. However, it could not tell whether or not the preloaded NOM was desorbed. DOC removals were not significantly different between the three ACs (Fig. 2S in the Supplementary Information). Because the initial MIB concentration was ~6 nmol/L (~1 μg/L), the concentration of the NOM that could be displaced with MIB would be estimated to be comparable to that concentration. However, the total NOM concentration in the experiments was >0.8 mg-C/L (> 1.5 μmol/L). The NOM that could be displaced with MIB was negligible compared to the total NOM, so if NOM displacement occurred, it would be difficult to detect.

3.2. *Adsorption irreversibility: the pore blockage effect*

Differences in MIB removals between the three sample types can be attributed to the irreversible adsorption (incomplete desorption) with direct site competition or pore blockage by NOM molecules. Irreversible adsorption occurs when MIB molecules are tightly adsorbed in small micropores with significant overlap with the pore wall potentials (Pelekani and Snoeyink 2000). However, almost complete reversibility was observed for SPAC, unlike PAC, at the same AC dosages, although the pore size distributions were not different between the two ACs (see Fig. 3S in the Supplementary

257 Information) as Ando et al. (2010) noted. Therefore, irreversible adsorption with direct site competition
258 cannot explain the incomplete desorption. As a remaining plausible mechanism, pore blockage was
259 proposed for the incomplete desorption of MIB. Pelekani and Snoeyink (1999) observed no desorption
260 of preloaded micropollutant (atrazine) on AC fibers containing primarily micropores and attributed
261 this phenomenon to a pore blockage mechanism wherein NOM molecules block access to, but do not
262 penetrate into, the primary micropores. Aschermann et al. (2018) also report that NOM adsorption
263 prevents the desorption of organic micropollutant from granular activated carbon (GAC). However, it
264 remained unanswered: whether internal or external pore blockage occurs. Internal pore blockage
265 occurs at the entrance of a micropore inside an AC particle, whereas external pore blockage occurs at
266 the outer interface area. If the pore blockage occurred internally, both SPAC and PAC would have
267 exhibited a similar pore blockage effect leading to similar irreversibility as the pore size distributions
268 are similar for both ACs. As a plausible mechanism, therefore, external pore blockage was proposed
269 for the irreversibility of MIB adsorption on AC.

270

271 3.3. *Effect of activated carbon particle size and NOM concentration*

272 Herein, the magnitude of irreversible adsorption was quantitatively evaluated using an index,
273 $\Delta_{Pre-Post}$, defined by the difference in MIB removal obtained by NOM-preloaded and NOM-post-
274 loaded ACs as follows:

275 $$\Delta_{Pre-Post} = R_{Pre} - R_{Post}$$

276 Where $\Delta_{Pre-Post}$ is a pore blockage index (dimensionless), R_{Pre} is the proportion of MIB remaining
277 (C/C_0) of the NOM-preloaded AC adsorption (dimensionless), and R_{Post} is the proportion of MIB
278 remaining (C/C_0) of the NOM-post-loaded AC adsorption (dimensionless).
279 The values of $\Delta_{Pre-Post}$ were calculated and shown in Fig. 4. The $\Delta_{Pre-Post}$ values were higher at

higher initial NOM concentrations (7 mg-C/L for SFA and 6 mg-C/L for SHA) and lower AC dosages (0.9 mg-C/L for SFA and 1.6 mg/L for SHA). This is reasonable because these experimental conditions should yield higher NOM loading per AC, resulting in a larger pore blockage effect. The NOM MWs used herein descend in the following order: SHA, SFA, and Chibaberi in terms of peak MW (Fig. 4S). When comparing the $\Delta_{Pre-Post}$ values at similar AC dosages in Fig.4, however, no such ordering trend was observed for their values between Chibaberi, SFA, and SHA. Therefore, the magnitudes of irreversible adsorption of MIB does not appear to be related to NOM MW. Actually, this result was somewhat unexpected, because it is widely accepted that pore blockage hindering intraparticle transport of micropollutant molecules in an AC particle is more effectively achieved by higher MW NOM (Pelekani and Snoeyink 2001). However, our result is in accordance with a very recent finding of Aschermann et al. (2019). They prepared two NOM fractions of low and high molecular weights and found that the impacts of the two fractions on organic micropollutant desorption were similar though pore blockage and micropollutant displacement occurred on both fractions. With reference to their paper, therefore, we feel our result is a possible outcome.

Overall, the $\Delta_{Pre-Post}$ values were lower for SPAC than PAC. SPAC with a smaller particle size showed higher MIB adsorption reversibility compared to the PAC samples. This is in agreement with the previous paper of Thacker et al. (1983), which stated that the quantity of adsorbate that can desorb from the GAC bed in response to decreased influent concentration increased with decreasing GAC particle size. It should be noted, however, that the particle sizes tested in the previous study are very different to those used herein. The higher reversibility for SPAC than PAC indicates that SPAC did not experience significant pore blockage effects, unlike PAC. This result is interesting because SPAC has been reported to exhibit higher NOM removal than PAC (Ando et al. 2010). NOM removals were actually higher for SPAC than for PAC (Fig. 2S in the Supplementary Information), and NOM loadings were higher on SPAC than on PAC. On the one hand, the high NOM loading on SPAC is explained by the Shell Adsorption in which NOM is adsorbed mainly in the vicinity of the outer surface of AC

306 particles (Ando et al. 2010, Ando et al. 2011). At a given AC dose, NOM is probably loaded to a lesser
307 extent on the outer surface area of SPAC particles compared to PAC particles because the total outer
308 particle surface area is much larger, and then external pore blocking probably occurs at a lower degree
309 for SPAC.

310

311 3.4. *NOM and MIB adsorption profiles on the activated carbon particles*

312 External pore blockages where NOM is loaded near the outer surface of AC particles, thereby blocking
313 the access of MIB molecules to the inner region was presented in the previous sections. Then, we tried
314 to achieve direct observation of the adsorbate distribution in AC particles using an isotope microscope
315 system and isotope-labeled adsorbates. ^{15}N-labeled EfOM was prepared and used as a NOM substitute.
316 The use of ^{15}N-labeled NOM was ideal, but it was not available, and its laboratory preparation was
317 impossible. However, we confirmed that the molecular weight distributions of the prepared ^{15}N-labeled
318 EfOM and the NOM are similar (Fig. 5S, SI). Figs. 5 and 6S (SI) show the isotope (^{15}N/^{14}N ratio) maps
319 of the AC particles obtained after the upsides of the AC particles were removed using ion beam
320 sputtering, exposing the particle interior (Matsui et al. 2014). The SEM pictures of the particles before
321 isotope microscopy measurements are also provided. The observed isotope ratios of EfOM-loaded ACs
322 ranged from 0.01 to 0.46, while the ^{15}N/^{14}N ratio of an entire AC particle is predicted to be ~0.1,
323 according to the ^{15}N/^{14}N ratio (0.018) of the EfOM, N/C ratio (0.10, w/w) of EfOM (Chen et al. 2009),
324 and carbon mass balance after adsorption. Fair agreement was found between the prediction and
325 calculation. The ratio of the non-loaded ACs was <0.01.

326

327 For 9 AC particles of the 10 observed, ^{15}N/^{14}N ratios were relatively high in the outer regions and in
328 the region with large macropore(s) as both regions were in direct contact with water during the
329 adsorption compared with the other regions which were not exposed to water. The ^{15}N/^{14}N ratio was,

however, not always high over the entire outer region for each particle, likely because some outer regions were removed during ion beam sputtering, exposing the particle interior. The differences in the $^{15}N/^{14}N$ ratios between the regions in contact with and shielded from water were approximately a factor of ≥2. Adsorption of NOM at the external region has been hypothesized implicitly or explicitly (Ando et al. 2010, Randtke and Snoeyink 1983), but this is the first evidence that EfOM (a type of NOM) mainly adsorbed near the outer surface area of AC particles and did not significantly diffuse inside the particle.

The $^{2}H/^{1}H$-ratios on ACs loaded with ^{2}H-labeled MIB are presented in Fig. 7S (SI), where the high ratio indicates significant MIB adsorption. The $^{2}H/^{1}H$-ratios in the NOM-preloaded AC particles were always low, and those of the NOM-post-loaded AC and NOM-free AC varied (the reason for the variation was not clearly known, but it might be due to the evaporation of MIB during the observation). Low $^{2}H/^{1}H$-ratios were observed in the NOM-preloaded ACs (Fig. 8S, SI) in all studied regions. Overall, NOM-preloaded AC particles showed significantly lower $^{2}H/^{1}H$-ratios than the NOM-post-loaded and NOM-free AC particles. These data support the external pore-blockage mechanism, which would cause irreversible adsorption on PAC.

3.5. *Changes in MIB removal by pulverization of NOM-preloaded activated carbon*

If pore blockage occurs at the external interface area of PAC particles, the pulverization of the PAC particles would break the blocking layer and enhance MIB adsorption because the inside of the PAC particles, which were not available for adsorption due to external pore blockage, became available. Then, the preloading-pulverization test was conducted to prove this. The results of MIB removal in the test are shown in Fig. 6. While the proportion of MIB remaining after contact with the preloaded-PAC was approximately 80%, that observed for the pulverized preloaded-PAC was 60%. Pulverization of

354 the preloaded-PAC particles actually enhanced MIB adsorption. Before concluding that the breakage
355 of external blocking layer was the main cause of the enhanced MIB removal, the possibilities of other
356 interpretations for the result were ruled out. One possibility (Interpretation A) is the occurrence of the
357 Shell Adsorption on MIB (Matsui et al. 2015). It has been reported that particle size reduction can
358 increase the adsorption capacity for hydrophobic compounds (including MIB) for some types of virgin
359 AC (not-preloaded AC) because adsorption mainly occurs at the external region of the AC particles.
360 For the tested PAC, particle size reduction without NOM-preloading did not increase the adsorption
361 capacity or MIB removal (Fig. 9S, SI). Thus, Interpretation A was denied. The other possibility
362 (Interpretation B), is the desorption of pore-blocking NOM by pulverization. However, Interpretation
363 B is not plausible because pulverization did not change the DOC. The DOC of the pulverized preloaded
364 PAC suspension was similar to that of the non-pulverized preloaded PAC (Fig. 10S, SI). Finally, the
365 MIB removal enhancement by pulverization of the preloaded PAC supported the external pore-
366 blocking mechanism as described previously.

367

368 **CONCLUSIONS**

369 The major conclusions of this study can be summarized as follows:

370 1) With small AC particle diameters (SPAC) and low NOM concentrations (0.9 and 1.6 mg-C/L), MIB
371 removals were similar between the NOM-preloaded, NOM-simultaneously loaded and NOM-post-
372 loaded ACs, and MIB adsorption was reversible for the MIB/NOM loading sequence. Similar results
373 were obtained at high AC dosages (> 10 mg/L) for PAC as well as SPAC. The reversibility of MIB
374 adsorption indicated direct site competition between MIB and NOM. Almost complete desorption of
375 MIB by NOM occurred until competitive adsorption equilibrium was reached.

376 2) At high NOM concentration or low PAC dosages, MIB removal was higher for NOM-post-loaded
377 AC compared to NOM-preloaded AC, and MIB adsorption was irreversible. The degree of

irreversibility was high on PAC compared to SPAC, although the two ACs were almost the same on pore size distribution. The lower degree of reversibility on PAC indicated external pore blockage via NOM adsorption at the outer interface area of PAC particles. External pore blockage by NOM on PAC was due to the smaller external particle surface area of PAC compared to SPAC, which would result in high NOM loading on the pores close to the outer interface area of AC particles.

3) EfOM as a substitute for NOM was labeled with ^{15}N and used for the adsorption experiments. The distribution of ^{15}N as a marker of EfOM inside the AC particles was directly observed using an isotope mapping system. Direct evidence was obtained for the high loading of EfOM at the external region of the PAC particles.

ACKNOWLEDGEMENTS

This study was supported by Grants-in-Aid for Scientific Research S (16H06362) and Grant-in-Aid for Challenging Research (Exploratory, 18K19866 and 19K21980) from the Japan Society for the Promotion of Science. A part of this work was the result of using research equipment shared in MEXT Project for promoting public utilization of advanced research infrastructure (JPMXS0410300120).

Appendix. Supplementary Information

Figs. 1S-9S are available in the online version at ######.

REFERENCES

399 Ando, N., Matsui, Y., Kurotobi, R., Nakano, Y., Matsushita, T. and Ohno, K. (2010) Comparison of natural organic matter
400 adsorption capacities of super-powdered activated carbon and powdered activated Carbon. Water Research 44(14), 4127-
401 4136.
402 Ando, N., Matsui, Y., Matsushita, T. and Ohno, K. (2011) Direct observation of solid-phase adsorbate concentration profile
403 in powdered activated carbon particle to elucidate mechanism of high adsorption capacity on super-powdered activated
404 carbon. Water Research 45(2), 761-767.
405 Aschermann, G., Neubert, L., Zietzschmann, F. and Jekel, M. (2019) Impact of different DOM size fractions on the
406 desorption of organic micropollutants from activated carbon. Water Research 161, 161-170.
407 Aschermann, G., Zietzschmann, F. and Jekel, M. (2018) Influence of dissolved organic matter and activated carbon pore
408 characteristics on organic micropollutant desorption. Water Research 133, 123-131.
409 Cai, Z., Wee, C. and Benjamin, M.M. (2013) Fouling mechanisms in low-pressure membrane filtration in the presence of
410 an adsorbent cake layer. Journal of Membrane Science 433(0), 32-38.
411 Chen, B., Nam, S.-N., Westerhoff, P.K., Krasner, S.W. and Amy, G. (2009) Fate of effluent organic matter and DBP
412 precursors in an effluent-dominated river: A case study of wastewater impact on downstream water quality. Water Research
413 43(6), 1755-1765.
414 Cook, D., Newcombe, G. and Sztajnbok, P. (2001) The application of powdered activated carbon for mib and geosmin
415 removal: predicting pac doses in four raw waters. Water Research 35(5), 1325-1333.
416 Delgado, L.F., Charles, P., Glucina, K. and Morlay, C. (2012) The removal of endocrine disrupting compounds,
417 pharmaceutically activated compounds and cyanobacterial toxins during drinking water preparation using activated
418 carbon—A review. Science of the Total Environment 435–436(0), 509-525.
419 Ding, L., Mariñas, B.J., Schideman, L.C., Snoeyink, V.L. and Li, Q. (2006) Competitive Effects of Natural Organic Matter:
420 Parametrization and Verification of the Three-Component Adsorption Model COMPSORB. Environmental Science &
421 Technology 40(1), 350-356.
422 Ding, L., Snoeyink, V.L., Mariñas, B.J., Yue, Z. and Economy, J. (2008) Effects of Powdered Activated Carbon Pore Size
423 Distribution on the Competitive Adsorption of Aqueous Atrazine and Natural Organic Matter. Environmental Science &
424 Technology 42(4), 1227-1231.
425 Ellerie, J.R., Apul, O.G., Karanfil, T. and Ladner, D.A. (2013) Comparing graphene, carbon nanotubes, and superfine
426 powdered activated carbon as adsorptive coating materials for microfiltration membranes. Journal of Hazardous Materials
427 261(0), 91-98.
428 Huang, C., VanBenschoten, J.E. and Jensen, J.N. (1996) Adsorption kinetics of MIB and geosmin. Journal American Water
429 Works Association 88(4), 116-128.
430 Huang, H., Schwab, K. and Jacangelo, J.G. (2009) Pretreatment for low pressure membranes in water treatment: a review.
431 Environmental Science & Technology 43(9), 3011-3019.
432 Karanfil, T., Dastgheib, S.A. and Mauldin, D. (2006) Exploring Molecular Sieve Capabilities of Activated Carbon Fibers
433 to Reduce the Impact of NOM Preloading on Trichloroethylene Adsorption. Environmental Science & Technology 40(4),
434 1321-1327.
435 Kilduff, J.E., Karanfil, T. and Weber, W.J. (1998) TCE adsorption by GAC preloaded with humic substances. Journal
436 American Water Works Association 90(5), 76-89.
437 Kilduff, J.E. and Wigton, A. (1999) Sorption of TCE by Humic-Preloaded Activated Carbon: Incorporating Size-Exclusion
438 and Pore Blockage Phenomena in a Competitive Adsorption Model. Environmental Science & Technology 33(2), 250-256.
439 Knappe, D.R.U., Matsui, Y., Snoeyink, V.L., Roche, P., Prados, M.J. and Bourbigot, M.-M. (1998) Predicting the Capacity
440 of Powdered Activated Carbon for Trace Organic Compounds in Natural Waters. Environmental Science & Technology
441 32(11), 1694-1698.
442 Li, Q., Mariñas, B.J., Snoeyink, V.L. and Campos, C. (2003a) Three-Component Competitive Adsorption Model for Flow-
443 Through PAC Systems. 1. Model Development and Verification with a PAC/Membrane System. Environmental Science &
444 Technology 37(13), 2997-3004.
445 Li, Q., Snoeyink, V.L., Campos, C. and Mariñas, B.J. (2002) Displacement Effect of NOM on Atrazine Adsorption by
446 PACs with Different Pore Size Distributions. Environmental Science & Technology 36(7), 1510-1515.
447 Li, Q., Snoeyink, V.L., Mariãas, B.J. and Campos, C. (2003b) Elucidating competitive adsorption mechanisms of atrazine
448 and NOM using model compounds. Water Research 37(4), 773-784.
449 Matsui, Y., Fukuda, Y., Inoue, T. and Matsushita, T. (2003) Effect of natural organic matter on powdered activated carbon
450 adsorption of trace contaminants: characteristics and mechanism of competitive adsorption. Water Research 37(18), 4413-
451 4424.
452 Matsui, Y., Fukuda, Y., Murase, R., Aoki, N., Mima, S., Inoue, T. and Matsushita, T. (2004) Micro-ground powdered
453 activated carbon for effective removal of natural organic matter during water treatment. Water Science & Technology:
454 Water Supply 4(4), 155-163.
455 Matsui, Y., Nakao, S., Sakamoto, A., Taniguchi, T., Pan, L., Matsushita, T. and Shirasaki, N. (2015) Adsorption capacities
456 of activated carbons for geosmin and 2-methylisoborneol vary with activated carbon particle size: Effects of adsorbent and
457 adsorbate characteristics. Water Research 85, 95-102.
458 Matsui, Y., Nakao, S., Taniguchi, T. and Matsushita, T. (2013) Geosmin and 2-methylisoborneol removal using superfine
459 powdered activated carbon: Shell adsorption and branched-pore kinetic model analysis and optimal particle size. Water

460 Research 47(8), 2873-2880.
461 Matsui, Y., Sakamoto, A., Nakao, S., Taniguchi, T., Matsushita, T., Shirasaki, N., Sakamoto, N. and Yurimoto, H. (2014)
462 Isotope Microscopy Visualization of the Adsorption Profile of 2-Methylisoborneol and Geosmin in Powdered Activated
463 Carbon. Environmental Science & Technology 48(18), 10897-10903.
464 Matsui, Y., Yoshida, T., Nakao, S., Knappe, D.R.U. and Matsushita, T. (2012) Characteristics of competitive adsorption
465 between 2-methylisoborneol and natural organic matter on superfine and conventionally sized powdered activated carbons.
466 Water Research 46(15), 4741-4749.
467 Najm, I.N., Snoeyink, V.L., Suidan, M.T., Lee, C.H. and Richard, Y. (1990) Effect of particle-size and background natural
468 organics on the adsorption efficiency of PAC. Journal American Water Works Association 82(1), 65-72.
469 Newcombe, G., Drikas, M. and Hayes, R. (1997) Influence of characterised natural organic material on activated carbon
470 adsorption: II. Effect on pore volume distribution and adsorption of 2-methylisoborneol. Water Research 31(5), 1065-1073.
471 Pelekani, C. and Snoeyink, V.L. (1999) Competitive adsorption in natural water: role of activated carbon pore size. Water
472 Research 33(5), 1209-1219.
473 Pelekani, C. and Snoeyink, V.L. (2000) Competitive adsorption between atrazine and methylene blue on activated carbon:
474 the importance of pore size distribution. Carbon 38(10), 1423-1436.
475 Pelekani, C. and Snoeyink, V.L. (2001) A kinetic and equilibrium study of competitive adsorption between atrazine and
476 Congo red dye on activated carbon: the importance of pore size distribution. Carbon 39(1), 25-37.
477 Randtke, S.J. and Snoeyink, V.L. (1983) EVALUATING GAC ADSORPTIVE CAPACITY. Journal American Water Works
478 Association 75(8), 406-413.
479 Summers, R.S., Knappe, D.R.U. and Snoeyink, V.L. (2011) Water quality and treatment: a handbook of community water
480 supplies. Edzwald, J.K. and American Water Works Association (eds), McGraw-Hill.
481 Summers, R.S. and Roberts, P.V. (1988) Activated carbon adsorption of humic substances: I. Heterodisperse mixtures and
482 desorption. Journal of Colloid and Interface Science 122(2), 367-381.
483 Thacker, W.E., Snoeyink, V.L. and Crittenden, J.C. (1983) Desorption of compounds during operation of GAC adsorption
484 systems. Journal of American Water Works Association 75(3), 144-149.
485 To, P.C., Mariñas, B.J., Snoeyink, V.L. and Ng, W.J. (2008) Effect of Pore-Blocking Background Compounds on the
486 Kinetics of Trace Organic Contaminant Desorption from Activated Carbon. Environmental Science & Technology 42(13),
487 4825-4830.
488 Wang, Y., Rao, G.Y. and Hu, J.Y. (2011) Adsorption of EDCs/PPCPs from drinking water by submicron-sized powdered
489 activated carbon. Water Science and Technology-Water Supply 11(6), 711-718.
490 Zoschke, K., Engel, C., Börnick, H. and Worch, E. (2011) Adsorption of geosmin and 2-methylisoborneol onto powdered
491 activated carbon at non-equilibrium conditions: Influence of NOM and process modelling. Water Research 45(15), 4544-
492 4550.
493

494

List of figures

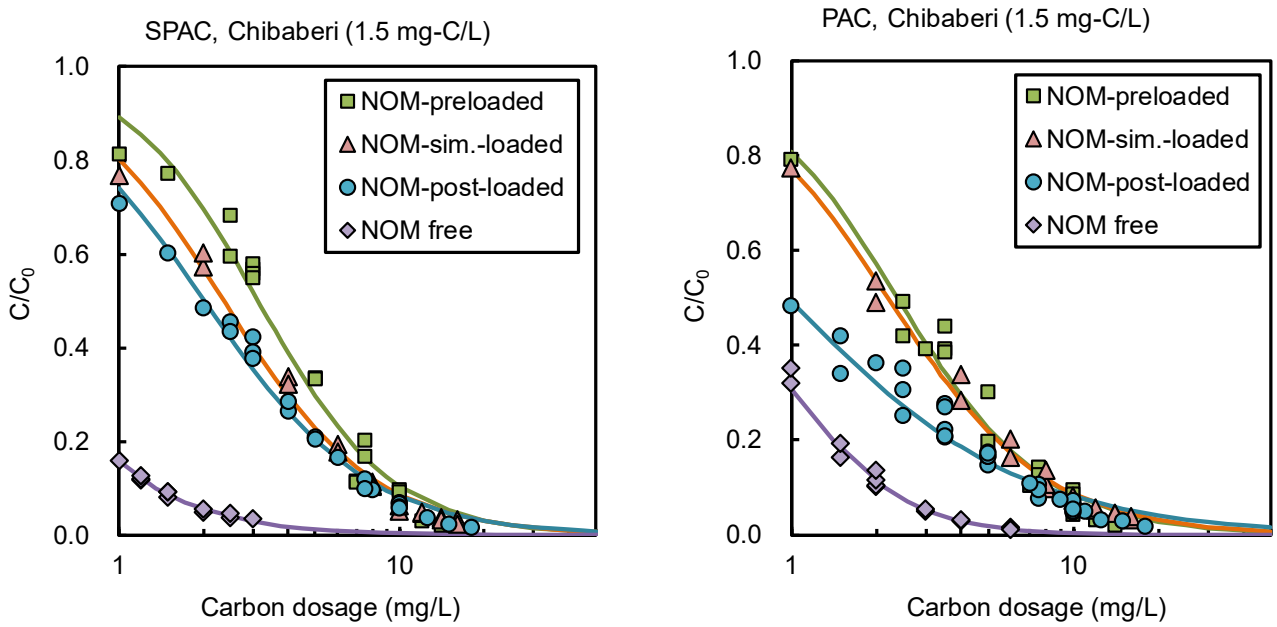

Figure1. Removal of MIB from the Chibaberi water samples as a function of AC dosage. The plots are experimental data and the lines are those obtained by fitting with Eqs. (1) or (3) provided in the SI.

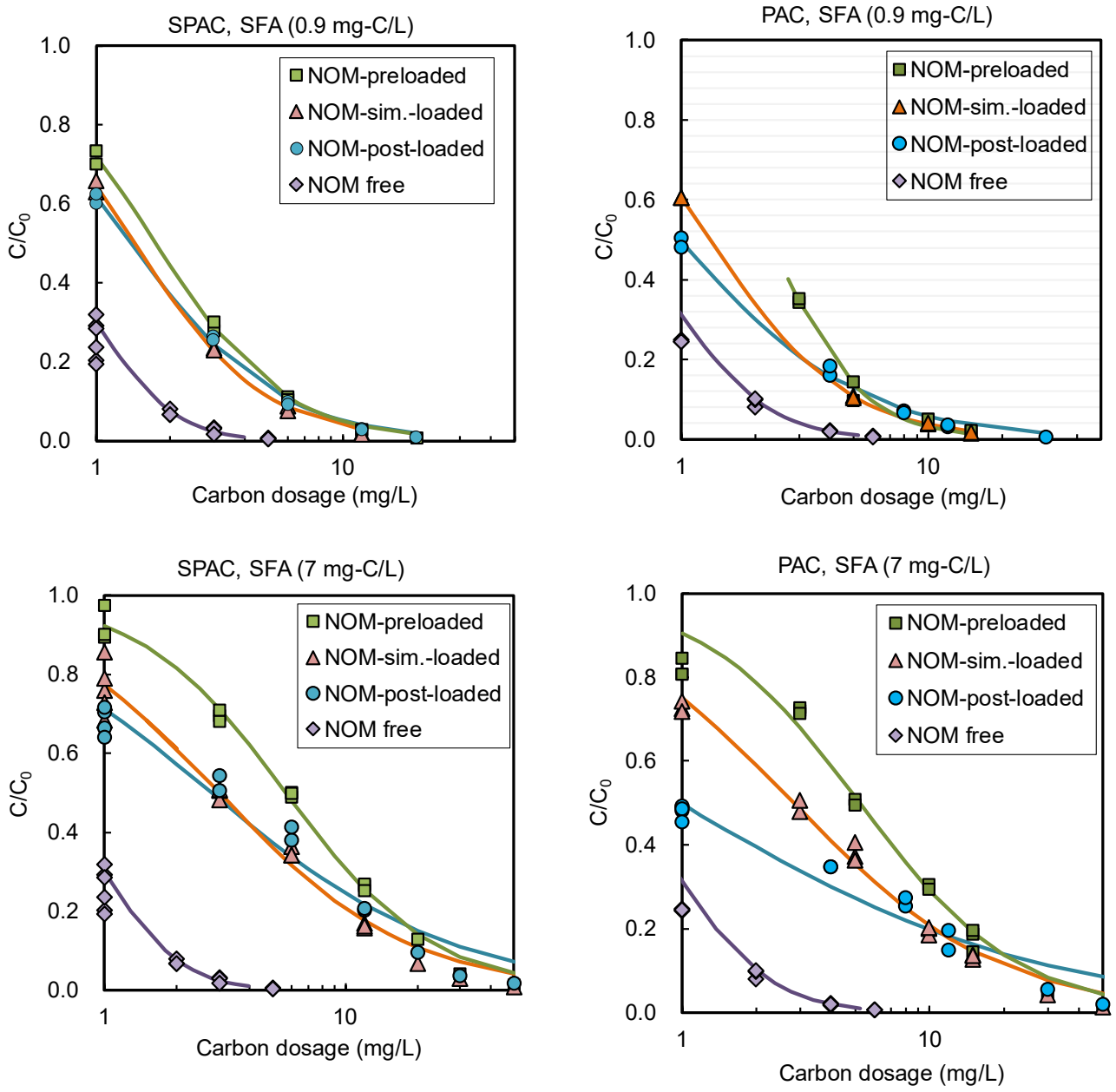

Figure 2. Removal of MIB from the SFA water samples as a function of AC dosage. The plots are experimental data and the lines are those obtained by fitting with Eqs. (1) or (3) provided in the SI. The upper and lower panels correspond to SFA concentrations of 0.9 and 7 mg-C/L, respectively.

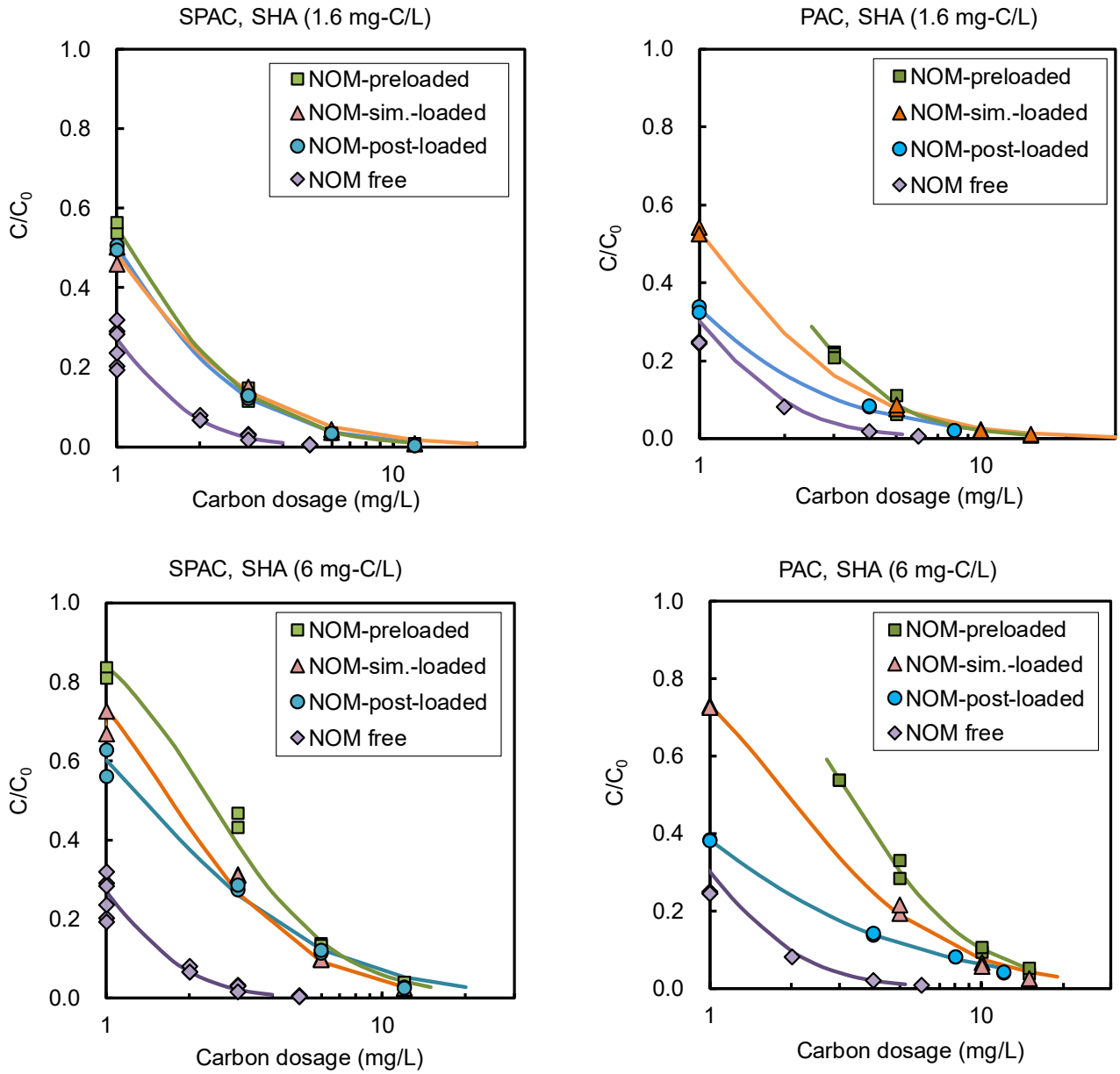

Figure 3. Removal of MIB from the SHA water samples as a function of AC dosage. The plots are experimental data and the lines are those obtained by fitting with Eqs. (1) or (3) provided in the SI. The upper and lower panels correspond to SHA concentrations of 1.6 and 6 mg-C/L, respectively.

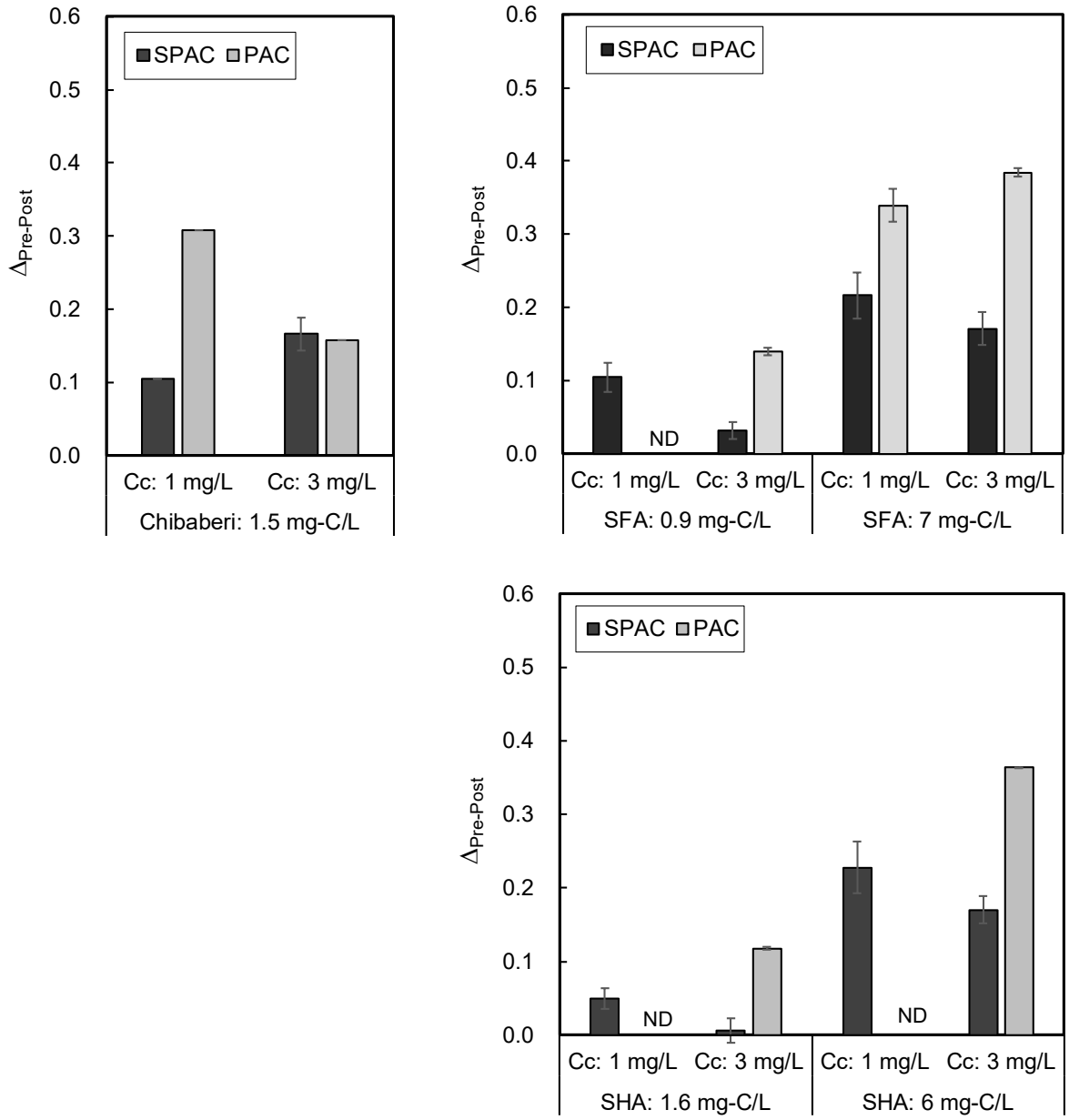

Figure 4. The $\Delta_{Pre-Post}$ values (difference in MIB removal obtained using NOM-preloaded and NOM-post-loaded carbons) used to evaluate effect of the pore blockage (irreversible adsorption of MIB). The upper left, upper right, and lower panels correspond to the Chibaberi, SFA, and SHA water samples, respectively. Cc indicates the AC dosage.

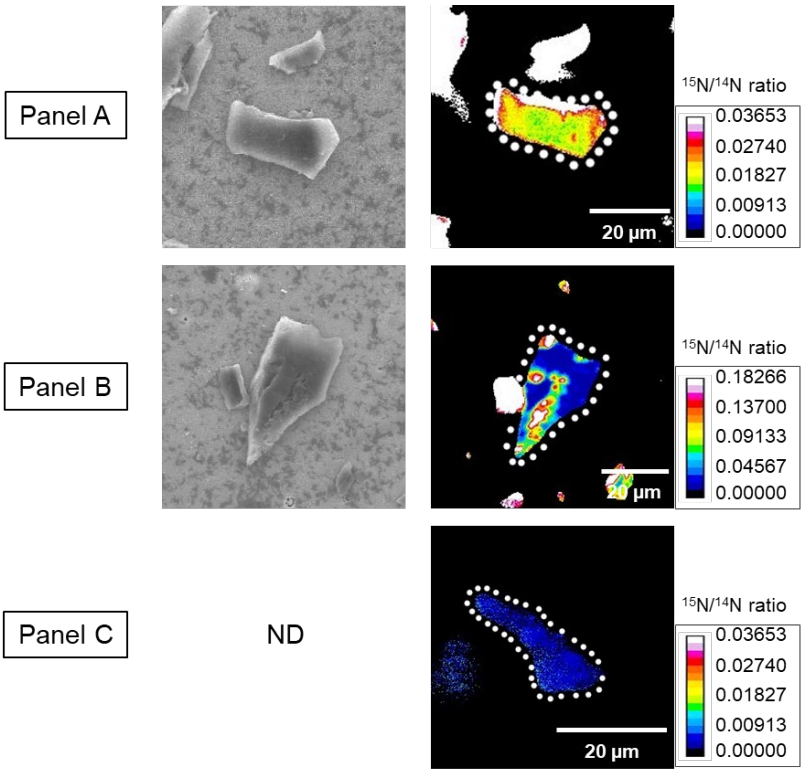

Figure 5. Left panels: LV-SEM images of AC particles loaded with ^{15}N-labeled EfOM before isotope microscopy measurements. Right panels: Isotopic maps ($^{15}N/^{14}N$ ratio) of the AC particles (non-target particles were identified after referring to the LV-SEM image and is depicted in white). Panels A and B: EfOM-loaded carbons. Panel C: EfOM-free AC. White dotted lines indicate the particle periphery. The LV-SEM images and isotopic maps of the other AC particles are provided in Fig. 5S (SI).

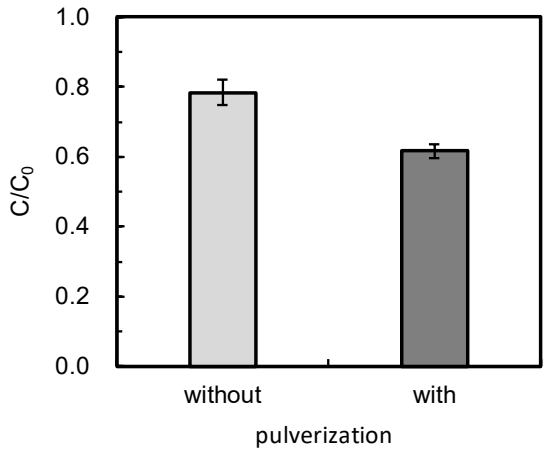

Figure 6. Comparison of MIB removal obtained using pulverized and non-pulverized NOM-preloaded AC particles with median dimeters of 5.8 and 18.8 μm, respectively (Chibaberi water, 1.5 mg/L DOC, 1 mg/L AC dosage).

Supplementary Information

Effects of Pre, Post, and Simultaneous Loading of Natural Organic Matter on 2-Methylisoborneol Adsorption on Superfine Powdered Activated Carbon: Reversibility and External Pore-blocking

Akiko Nakayama[1], Asuka Sakamoto[1], Taku Matsushita[2], Yoshihiko Matsui[2,]*, and Nobutaka Shirasaki[2]

[1]Graduate School of Engineering, Hokkaido University

[2]Faculty of Engineering, Hokkaido University

* Corresponding author. Phone: +81-11-706-7280.

E-mail address: matsui@eng.hokudai.ac.jp

Data analysis

Micropollutant isotherms obtained by batch adsorption tests in the presence of NOM vary with the initial micropollutant concentration (Knappe et al. 1998). However, the proportion of micropollutant remaining (C/C_0, where C is the concentration and subscript zero indicates the initial concentration) after AC adsorption in the presence of NOM is a function of AC dosage and independent of the initial micropollutant concentration. In the MIB adsorption tests, the initial concentrations were adjusted to 1000 ng/L, but there was variation from 800 to 1290 ng/L. To prevent any complications from the varied initial concentration, the experimental adsorption data were expressed in the plot of C/C_0 vs. AC dosage instead of isotherm plots. The curve of C/C_0 as a function of AC dosage can be described mathematically using the two parameter equation (Qi et al. 2007, Zoschke et al. 2011).

$$\frac{C}{C_0} = \frac{1}{A{C_\mathrm{C}}^{1/n} + 1} \tag{1}$$

where C is concentration of the removal-target micropollutant (ng/L); C_C is the AC dosage (mg/L); the subscript 0 (zero) indicates the initial concentration of the removal-target micropollutant; and A and n are model parameters.

This equation was derived from ideal adsorption solution theory (IAST) simplification with the following assumptions: 1) the adsorbed amount of competing NOM is greater than the competing NOM remaining in the solution and 2) the competing NOM dominates surface loading in the AC pores over that of the micropollutant. Qi et al. (2007) discussed how these assumptions affect the estimation of C/C_0 values and showed that the estimations were within reasonable errors (15%).

Eq. (1) was fitted to the experimental data under the minimum error criteria and the model parameters were optimized.

$$\sum \left(\frac{C}{C_0}_{observation} - \frac{C}{C_0}_{calculation} \right)^2 \tag{2}$$

The curve of C/C_0 as a function of AC dosage in single solute system (MIB in organic-free water) was fitted to the following equation, which was derived from the Freundlich isotherm and the mass balance equation in the batch adsorption system.

$$\frac{C}{C_0} + \frac{k_\mathrm{F}\, C_\mathrm{C}}{{C_0}^{1-\frac{1}{n_\mathrm{F}}}} \left(\frac{C}{C_0} \right)^{\frac{1}{n_\mathrm{F}}} - 1 = 0 \tag{3}$$

where k_F and n_F are the Freundlich constant and exponent, respectively.

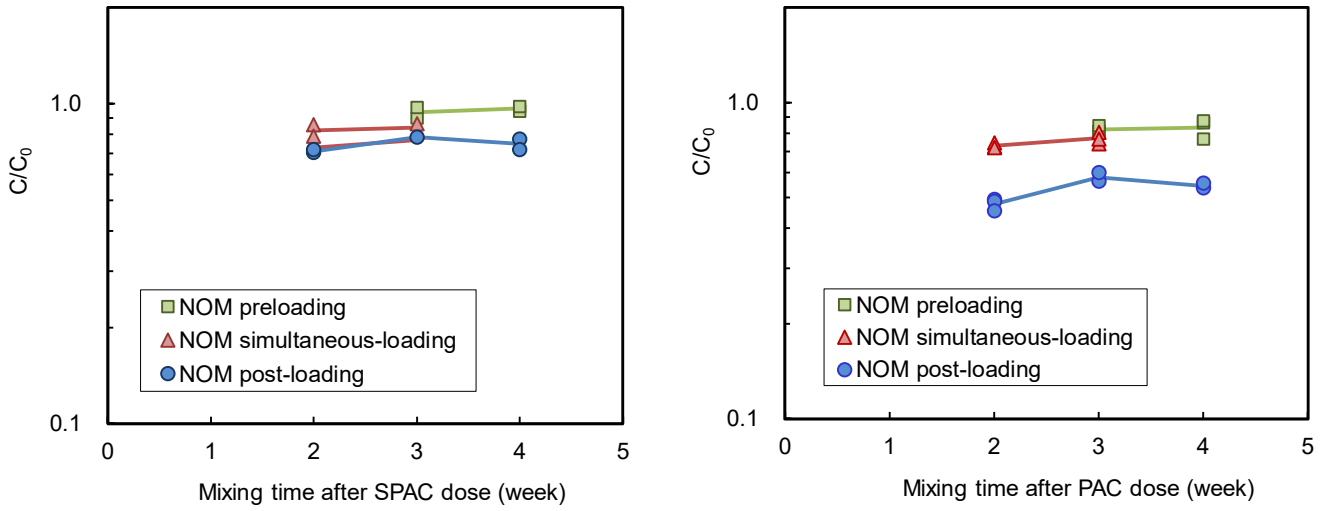

Figure 1S. Change in the MIB concentration during mixing. The left panel shows the SPAC results and the right panel is the PAC results. C/C_0 indicates the proportion of MIB remaining. SFA (6 mg-C/L) was used as the NOM. AC dosages were 1 mg/L. In the NOM preloading test, MIB was added to the NOM-AC solution, which had been shaken for one week. The MIB-NOM-AC mixture was shaken for 3 weeks. The MIB concentrations in the water phase were measured after 2 weeks (total mixing time: 3 weeks) and after 3 weeks (total mixing time: 4 weeks). In the NOM simultaneous-loading tests, the MIB concentrations in the water phase were measured after both 2 and 3 weeks. In the NOM post-loading test, NOM was added to a MIB-AC solution that had been shaken for one week at 6 mg-C/L. The NOM-MIB-AC solution was shaken for 3 weeks, and the MIB concentrations in the water phase were measured after 1 week (total mixing time: 2 weeks), 2 weeks (total mixing time: 3 weeks), and 3 weeks (total mixing time: 4 weeks).

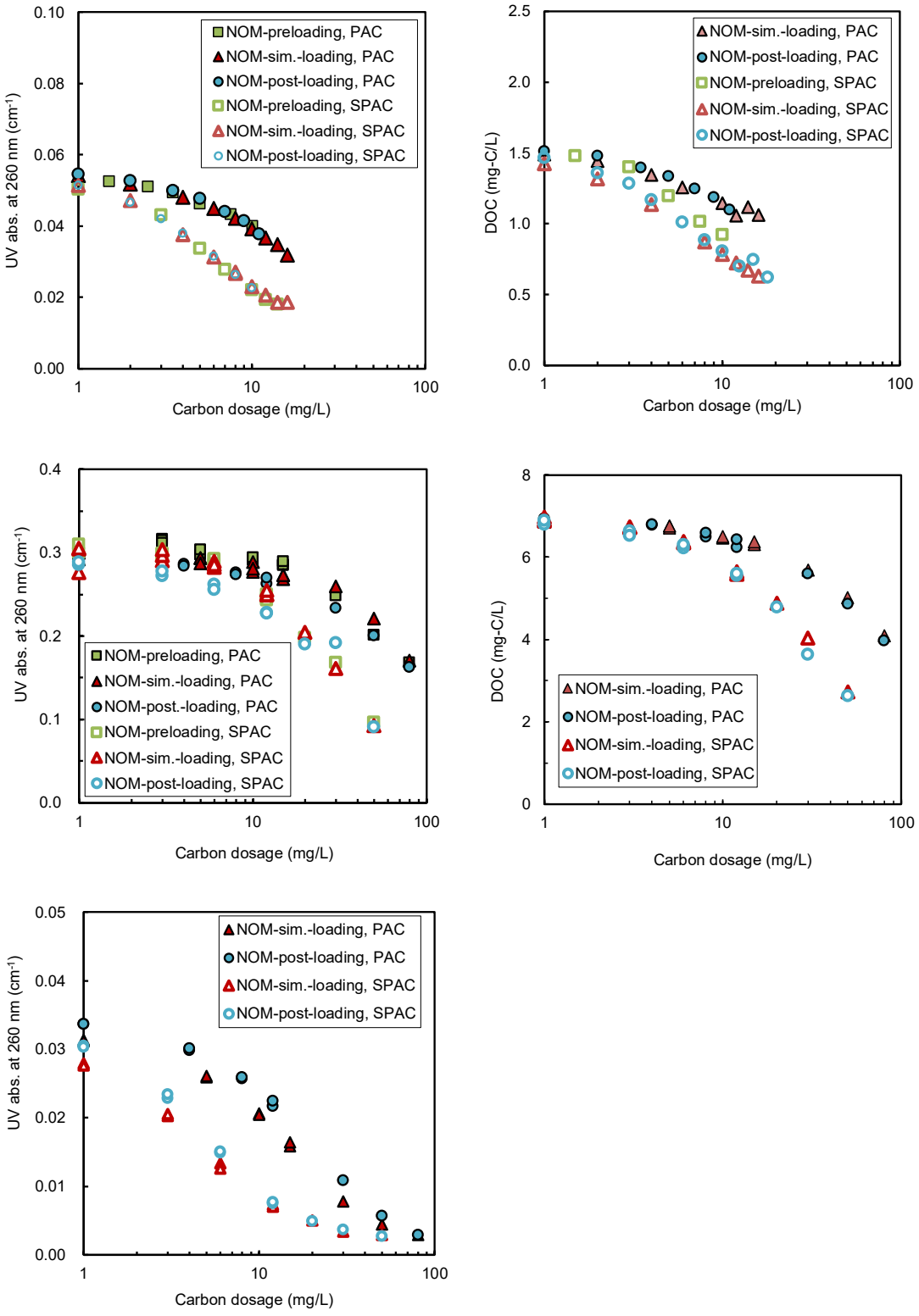

Figure 2S. Changes in the NOM concertation in terms of UV absorbance (left panels) and DOC (right panel) as a function of AC dosage. The upper panel shows the results of Chibaberi water (initial DOC of 1.5 mg-C/L). The middle and lower panels show the SFA water (7 and 0.9 mg/L, respectively) results.

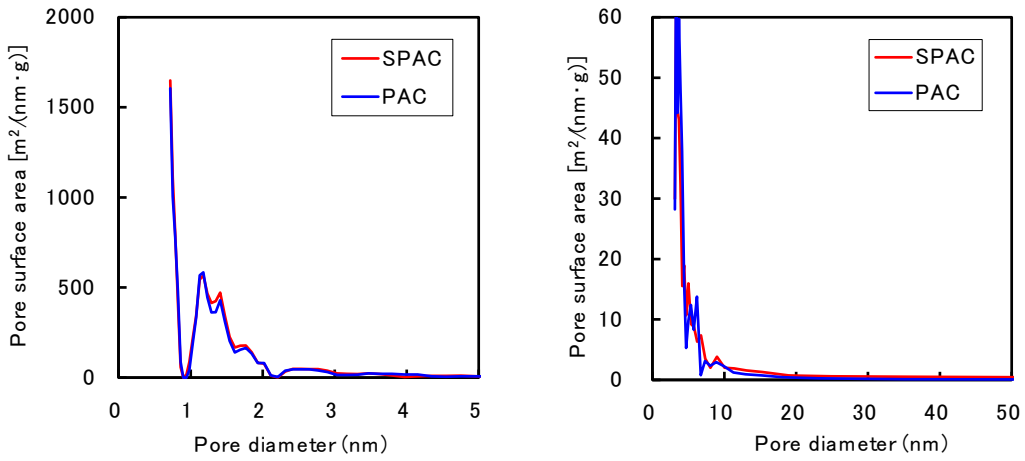

Figure 3S. Micropore (left panel) and mesopore (right panel) size distributions of SPAC and PAC.

The pore size distributions were determined using the nitrogen gas adsorption-desorption method (Autosorb-iQ, Quantachrome Instruments, Kanagawa, Japan). Isotherm data for nitrogen gas desorption at 77.4 K were analyzed using the Barrett-Joyner-Halenda (BJH) method for the mesopore region (pore diameter 2–20 nm) and with the density functional theory (DFT) for the micropore region (pore diameter 0.7–2 nm) (ASiQwin, ver.3.01, Quantachrome Instruments).

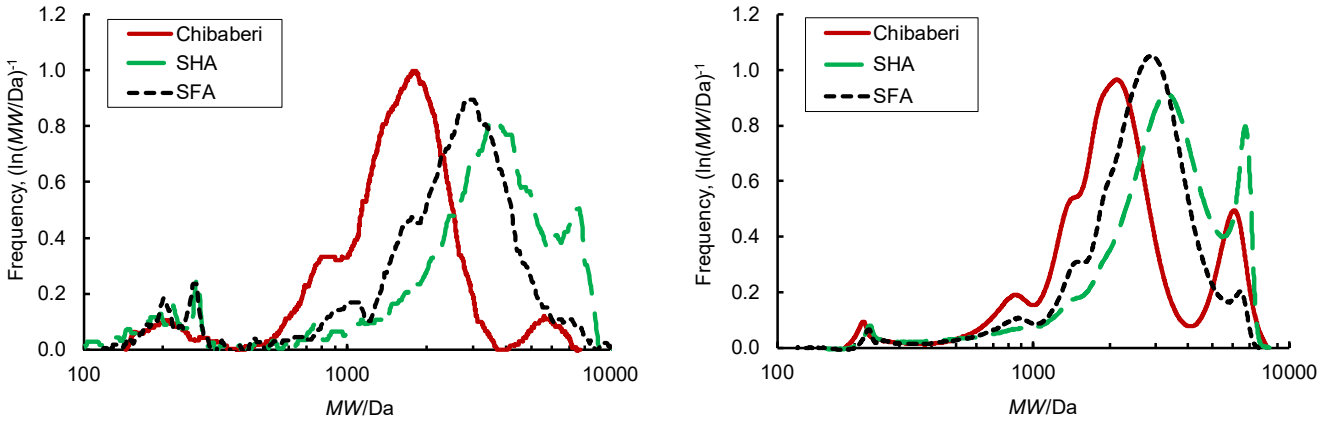

Figure 4S. Molecular weight distributions of Chibaberi, SHA, and SFA water NOM in terms of DOC (left panel) and UV absorbance at 260 nm (right panel).

The NOM MW distributions were determined using high performance size exclusion chromatography (HP1100 Agilent Technologies, Inc., CA, USA) with a packed column of GL-P252 (Hitachi, Ltd., Japan). Eluent was 0.02 M Na_2HPO_4 + 0.02 M KH_2PO_4. Polystyrene sulfonate (weight-average MWs of 1920, 5180, and 6130 Da) and salicylic acid (138 Da) were used for calibration (Zhou et al. 2000). The UV260 absorbance and DOC (Model 810 Turbo; GE Analytical Instruments, Boulder Co.) of the HPSEC column effluent were continuously measured.

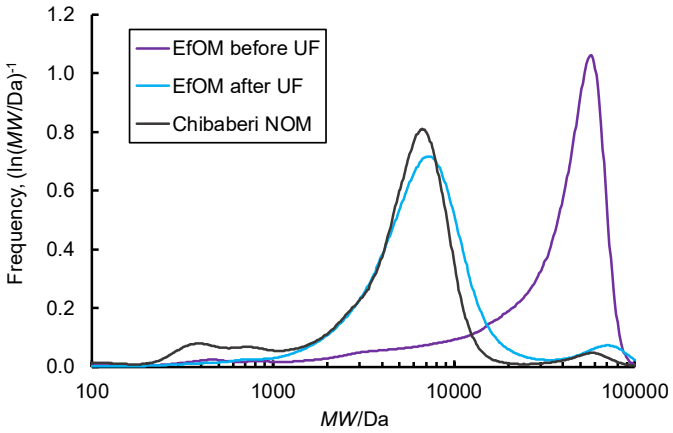

Figure 5S. Comparison of molecular weight distributions between EfOM and Chibaberi NOM. The NOM MW distributions were determined using high performance size exclusion chromatography (HP1100 Agilent Technologies, Inc., CA, USA) with a packed column of TSK HW50S (Tosoh Corp., Japan). To measure the macromolecular components in raw EfOM, a different packed column was used than the one shown in Figure 4. Therefore, the absolute value of molecular weight is different from that of Figure 4S. Eluent was 0.00845 M Na_2HPO_4 + 0.018 M KH_2PO_4. Polystyrene sulfonates (weight-average MWs of 3610, 6520, and 29100 Da) were used for calibration. DOC (Model 810 Turbo; GE Analytical Instruments, Boulder Co.) of the HPSEC column effluent were continuously measured.

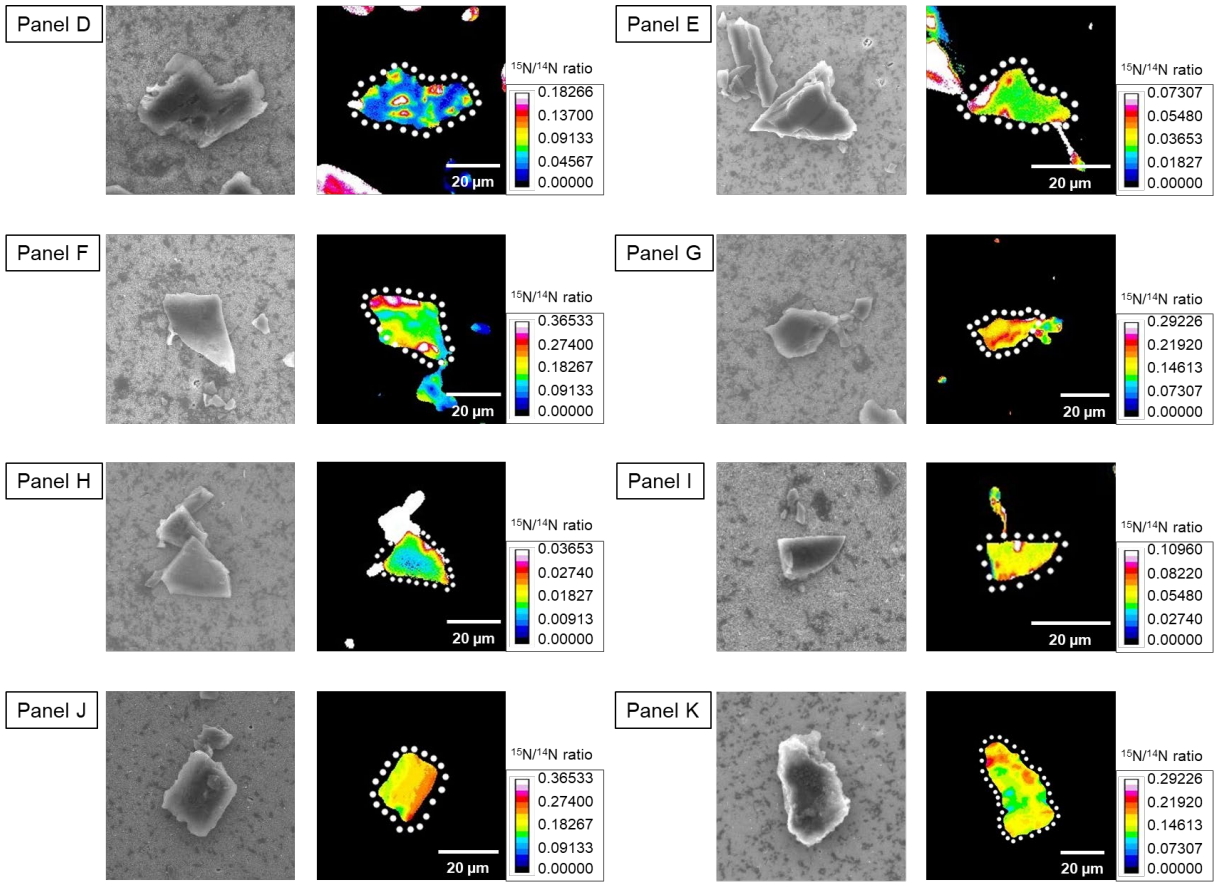

Figure 6S. Left panels: LV-SEM images of AC particles loaded with ^{15}N-labeled EfOM before isotope microscopy measurements. Right panels: Isotopic maps ($^{15}N/^{14}N$ ratio) of the obtained AC particles (background identified after referring to the LV-SEM image and is depicted in black/white). Panel D to K: EfOM-loaded carbons. White dotted lines indicate the particle periphery. Except Panel J, $^{15}N/^{14}N$ ratios were high in the outer regions of the particle, which was in direct contact with water, and in regions with very large pores.

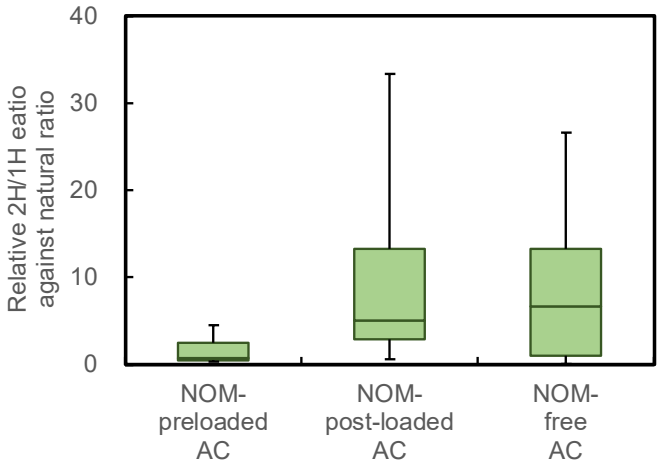

Figure 7S. Average $^{2}H/^{1}H$ ratios in the AC particles loaded with ^{2}H-labeled MIB. The boxplots present 13, 12 and 9 sample statistics of NOM-preloaded, NOM post-loaded and NOM-free ACs, respectively - the minimum, the lower quartile, the median, the upper quartile and the maximum.

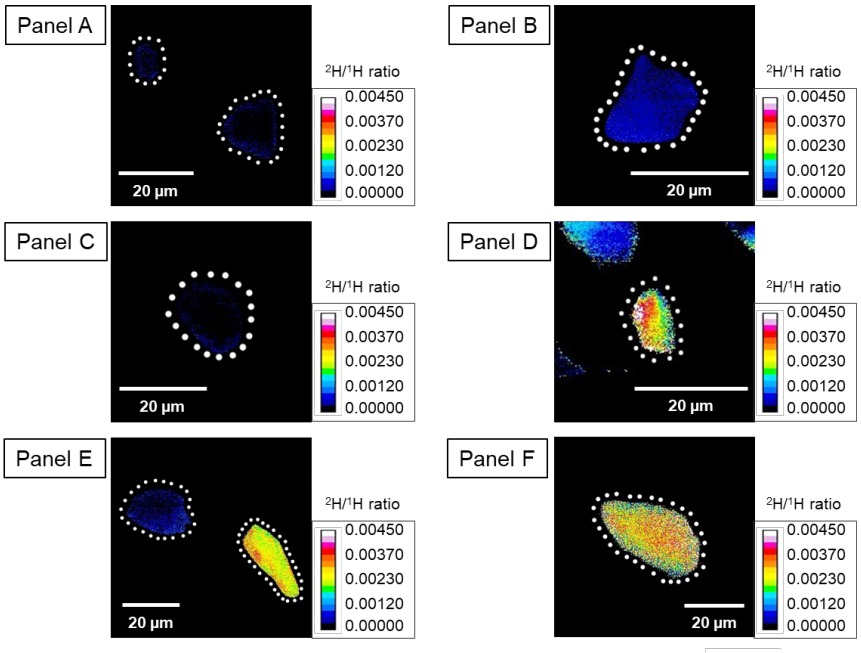

Figure 8S. Isotopic maps ($^{2}H/^{1}H$ ratio) of the AC particles loaded with ^{2}H-labeled MIB. Panels A and B: NOM-preloaded AC. Panels C and D: NOM-post-loaded AC. Panels E and F: NOM-free AC. White dotted lines indicate the particle periphery. Chibaberi water with 1.4 mg/L DOC was used as NOM water and the AC dosage was 1 mg/L.

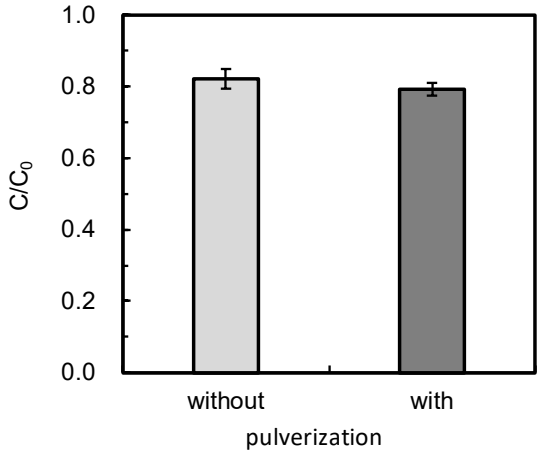

Figure 9S. Comparison of the MIB removal obtained using pulverized and non-pulverized AC particles with median dimeters of 6.7 and 21 μm, respectively (Chibaberi water with 1.4 mg/L DOC, AC dosage of 1 mg/L).

Experimental procedure: after a specified amount of PAC was added to a bottle containing a NOM-free solution (5 L, the ionic composition was same as the NOM water), the PAC was recovered and pulverized using the same procedure as the preloading-pulverization test. A portion of the PAC sludge containing the pulverized or non-pulverized PAC was added to a vial containing 140 mL of NOM solution (Chibaberi water) at 1.5 mg/L DOC, and shaken for one week. Subsequently, a small amount of high concentration MIB solution (10 mL, 15 μg/L) was added to the vial containing the NOM-preloaded PAC so that the initial MIB concentration was approximately 1000 ng/L. The vials were then shaken for two weeks and the MIB concentration in the water phase was determined.

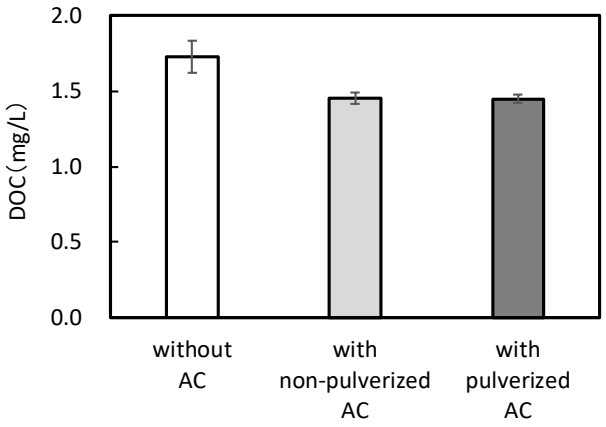

Figure 10S. DOC concentrations in the water with/without contact with pulverized/non-pulverized PAC.

Experimental procedure: Chibaberi water was used as the NOM solution. The NOM-loaded PAC sludge particles were obtained in the preloading-pulverization test and pounded in a mortar. After the NOM-loaded PAC particles were pulverized for 10 min using a mortar and pestle, ultrapure water (Milli-Q Advantage) was added. After thorough mixing for approximately 5 min, the water was passed through a membrane filter and the DOC concertation was determined. A control sample was prepared using the same procedure except that the PAC was not pulverized. Another control sample was prepared by the following procedure: a 10-mL NOM solution without the NOM-loaded PAC particles was obtained by filtering a portion of the 5-L water after the one-week adsorption in the preloading-pulverization test. The water was transferred to a mortar (10 mL) and placed under vacuum for 3 h for evaporation. Then, 10 mL of ultrapure water was added to the mortar, mixed, and the DOC concertation was determined.

References

Knappe, D.R.U., Matsui, Y., Snoeyink, V.L., Roche, P., Prados, M.J. and Bourbigot, M.-M. (1998) Predicting the Capacity of Powdered Activated Carbon for Trace Organic Compounds in Natural Waters. Environmental Science & Technology 32(11), 1694-1698.

Qi, S., Schideman, L., Marinas, B.J., Snoeyink, V.L. and Campos, C. (2007) Simplification of the IAST for activated carbon adsorption of trace organic compounds from natural water. Water Research 41(2), 440-448.

Zhou, Q., Cabaniss, S.E. and Maurice, P.A. (2000) Considerations in the use of high-pressure size exclusion chromatography (HPSEC) for determining molecular weights of aquatic humic substances. Water Research 34(14), 3505-3514.

Zoschke, K., Engel, C., Börnick, H. and Worch, E. (2011) Adsorption of geosmin and 2-methylisoborneol onto powdered activated carbon at non-equilibrium conditions: Influence of NOM and process modelling. Water Research 45(15), 4544-4550.